THE JOURNAL OF PHYSICAL CHEMISTRY Letters

Letter

pubs.acs.org/JPCL

Direct Observation of Ferroelectric Domains in Solution-Processed $CH_3NH_3PbI_3$ Perovskite Thin Films

Yasemin Kutes,[†,∥] Linghan Ye,[†,∥] Yuanyuan Zhou,[‡,∥] Shuping Pang,[§] Bryan D. Huey,*[,†] and Nitin P. Padture*[,‡]

[†]Department of Materials Science and Engineering, University of Connecticut, Storrs, Connecticut 06269, United States

[‡]School of Engineering, Brown University, Providence, Rhode Island 02912, United States

[§]Qingdao Institute of Bioenergy and Bioprocess Technology, Chinese Academy of Sciences, Qingdao 266101, People's Republic of China

Supporting Information

ABSTRACT: A new generation of solid-state photovoltaics is being made possible by the use of organometal-trihalide perovskite materials. While some of these materials are expected to be ferroelectric, almost nothing is known about their ferroelectric properties experimentally. Using piezoforce microscopy (PFM), here we show unambiguously, for the first time, the presence of ferroelectric domains in high-quality β-$CH_3NH_3PbI_3$ perovskite thin films that have been synthesized using a new solution-processing method. The size of the ferroelectric domains is found to be about the size of the grains (~100 nm). We also present evidence for the reversible switching of the ferroelectric domains by poling with DC biases. This suggests the importance of further PFM investigations into the local ferroelectric behavior of hybrid perovskites, in particular *in situ* photoeffects. Such investigations could contribute toward the basic understanding of photovoltaic mechanisms in perovskite-based solar cells, which is essential for the further enhancement of the performance of these promising photovoltaics.

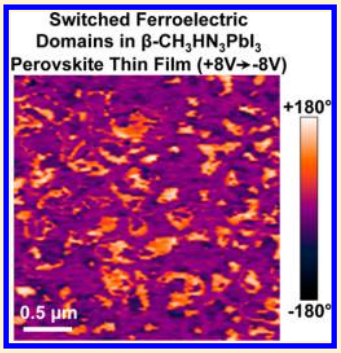

SECTION: Energy Conversion and Storage; Energy and Charge Transport

The past five years has witnessed a surge of interest in organometallic trihalide perovskites, which are at the heart of the new solid-state excitonic solar cells.[1−3] While these perovskites are a family of materials with the general formula $(RNH_3)MeX_3$ (R is an organic group, Me is Pb or Sn, and X is a halogen I, Br, or Cl), methylammonium (MA) lead triiodide ($CH_3NH_3PbI_3$ or $MAPbI_3$) in particular has attracted the most attention since it was first applied as light absorber in mesoscopic solar cells.[4,5] Since then the power conversion efficiency (PCE) of $MAPbI_3$-based solar cells have shot up dramatically, which now exceeds 19%.[6] This rapid rise in the performance is the result of the innate desirable properties of $MAPbI_3$, including favorable direct band gap, large absorption coefficient, high carrier mobilities, and long carrier-diffusion lengths.[4] While the optical, electrical, electronic, and optoelectronic properties of $MAPbI_3$ perovskites have been studied in great detail,[7−11] direct evidence of their ferroelectric properties is almost completely lacking.

$MAPbI_3$ crystallizes in a tetragonal perovskite crystal structure (β-$MAPbI_3$) at room temperature, containing the polarizable organic cation $CH_3NH_3^+$ in 12-fold cuboctahedral coordination.[12] Perovskite β-$MAPbI_3$ belongs to the *4mm* point group and *I4/mcm* space group, and thus, it is expected to be ferroelectric.[12,13] In this context, Stoumpos et al.[12] have measured current (I)−voltage (V) response of bulk single-crystals of β-$MAPbI_3$ using the four-probe method, and they observe hysteretic behavior suggesting bulk ferroelectric behavior. However, β-$MAPbI_3$ thin films used in solar cells are known to comprise nano- and microscale grains/domains of varying crystallinity,[14] and thus, it is important to characterize and understand local ferroelectric domains in β-$MAPbI_3$ thin films, which could influence the performance of solar cells based on these perovskites in several ways. First, the ferroelectric effect induces polarization of the lattice, which in turn can enhance charge separation and concomitant longer carrier lifetimes.[15] Second, open circuit voltages above the band gap are possible due to the ferroelectric effect.[16] Finally, the commonly observed hysteresis and rate dependence in the photovoltaic response (current density−voltage or J−V) of $MAPbI_3$-based solar cells[17,18] could be, in part, due to the ferroelectric effect.

In this context, we have investigated smooth, dense β-$MAPbI_3$ thin films using piezoforce microscopy (PFM)[19] — an ideal tool for probing local ferroelectric response at the domain scale. PFM is based on atomic force microscopy (AFM), where an AC electric field is applied to a scanning conducting probe in contact with a ferroelectric thin film surface. Since all ferroelectric materials are also piezoelectric,[13] the region in contact with the tip mechanically vibrates, which is simultaneously detected by the AFM during scanning. The

Received: August 11, 2014
Accepted: September 15, 2014
Published: September 15, 2014

   dx.doi.org/10.1021/jz501697b | *J. Phys. Chem. Lett.* 2014, 5, 3335−3339

phase difference between the piezoactuation and the applied AC field is then used to detect ferroelectric domain orientations, while the amplitude reveals domain wall positions. Superimposing a DC voltage on the domain-mapping AC signal can be used to switch the domains *in situ* during scanning.[20] Similarly, as employed here, poling can be achieved during scans applying continuous DC-biases (or pulse patterns), which are then alternated with zero DC-bias PFM domain mapping scans.[19,20] In this manner, we have directly imaged domains and domains walls in β-$MAPbI_3$ thin films directly using PFM, and an attempt to switch the ferroelectric domains reversibly using scanning DC biases has been successful.

Figure 1A is a schematic diagram showing a new solution-processing method—successive spin-coating/annealing (SSCA)—used in this study to prepare β-$MAPbI_3$ thin films. This method, which is a variation of the conventional two-step process used to synthesize β-$MAPbI_3$ thin films for planar solar cells,[21] uses multiple iterations of rapid spin-coating of MAI on the PbI_2 layer and annealing steps. (See Supporting Information for all the experimental procedures involving synthesis, characterization, and PFM.)

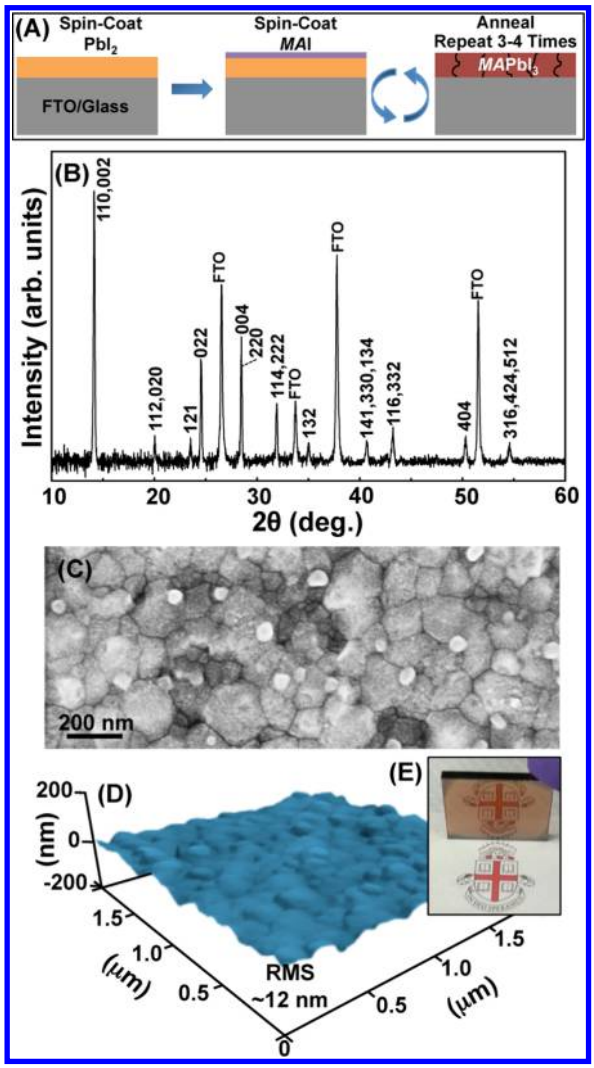

Figure 1. (A) Schematic diagram showing the SSCA solution-processing method. Characteristics of top surface of as-processed β-$MAPbI_3$ thin films: (B) indexed XRD pattern (peaks from FTO substrate are marked), (C) SEM micrograph, and (D) AFM scan ($2 \times 2\ \mu m^2$) showing RMS roughness of ~12 nm. (E) Photograph showing the mirror-like reflective nature of the smooth as-processed β-$MAPbI_3$ thin film ($25 \times 25\ mm^2$).

Figure 1B is an indexed X-ray diffraction (XRD) pattern of the resulting thin films (~100 nm thickness) showing phase-pure tetragonal β-$MAPbI_3$ perovskite. Figure 1C is a scanning electron micrograph (SEM) showing the dense, coarse-grained nature of the polycrystalline β-$MAPbI_3$ thin film. The grain size is estimated at ~100 nm, suggesting that most grains span the thickness of the thin film. The smooth surface topography in the β-$MAPbI_3$ thin film is clearly evident from the AFM image (noncontact mode) in Figure 1D, and analysis of local surface topography data reveals a RMS roughness of ~12 nm. Furthermore, the β-$MAPbI_3$ thin film surface looks mirror-like and "shiny" to the naked eye over a large area (Figure 1E).

The desirable attributes in these β-$MAPbI_3$ perovskite thin films—phase-pure, high crystallinity, dense, coarse-grained, smooth—are due to the new SSCA protocol (Figure 1A), allowing us to perform careful PFM experiments. In SSCA, successive MAI spin-coating/annealing steps replace the dipping, or the single spin-coating, step in the conventional two-step process. The rapid spin-coating of the MAI solution allows quick drying of an extremely thin, dense film of MAI. The subsequent heat-treatment (150 °C) results in the solid-state conversion reaction: $PbI_2 + MAI \rightarrow MAPbI_3$. However, the amount of MAI is not sufficient for the conversion of the full thickness of the PbI_2 thin film, as evinced by the yellow color of the thin film observed after the first cycle (not shown here). Repeating the MAI spin-coating/annealing steps 3−4 times results in the full conversion of the entire PbI_2 thin film into phase-pure β-$MAPbI_3$. Thus, promoting solid-state reaction between MAI and PbI_2 step-by-step, while minimizing the presence of liquid solution during each repeat cycle, is key to obtaining high quality β-$MAPbI_3$ thin films reported here. In contrast, the conventional MAI solution single dipping, or spin-coating, process for the fabrication of planar solar cells allows the conversion reaction to occur in the presence of the solution over a relatively long period of time, forming relatively rough thin films with interconnected β-$MAPbI_3$ particles and voids.[21,22]

Figure 2A is a $1 \times 1\ \mu m^2$ AFM image (contact mode) showing the representative topography for the β-$MAPbI_3$ thin film. Bright contrast indicates protrusions and depressions in the range ±20 nm, respectively, revealing grain sizes on the order of 100−200 nm, which is consistent with the SEM observations (Figure 1C). Figure 2B,C are simultaneously acquired PFM amplitude- and phase-contrast images, respectively. Ferroelectric domains in the β-$MAPbI_3$ thin films are clearly indicated by the complete 180° phase-contrast observed throughout Figure 2C (+90° to −90°). These out-of-phase and in-phase signals represent regions with piezoresponse vector components oriented into and out of the surface, respectively. Null contrast in the amplitude image (Figure 2B) identifies the intermediate domain wall locations.

PFM contrast can be susceptible to topographic artifacts, as with any AFM-based measurement technique. If similar contrast occurs only for specific slopes or curvatures, this usually indicates tip−sample convolution artifacts. Accordingly, the piezoresponse has been overlaid on a three-dimensional map of the topography (Figure 2D,E), where the color contrast displays the amplitude and phase of the piezoactuation vector with the same color scales as in Figure 2B,C, respectively. The piezoresponse (especially the phase) is clearly independent of

dx.doi.org/10.1021/jz501697b | J. Phys. Chem. Lett. 2014, 5, 3335−3339

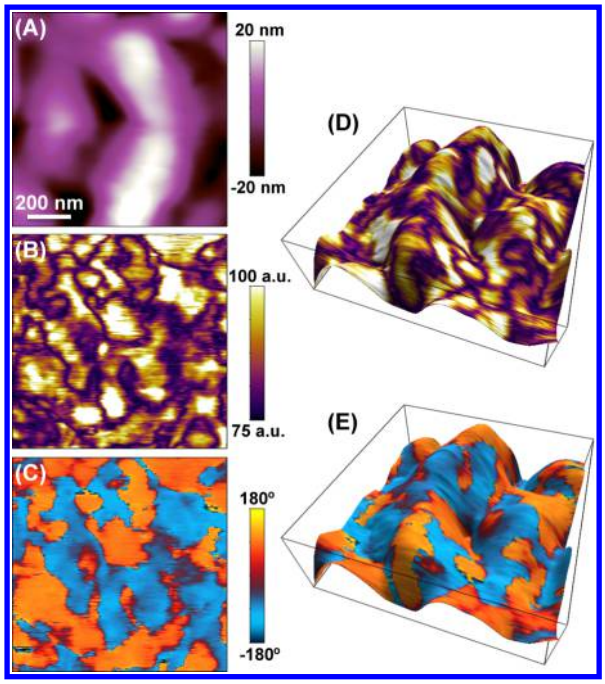

Figure 2. AFM and PFM images of as-processed β-$MAPbI_3$ thin film (1 × 1 μm^2): (A) AFM topography, (B) PFM amplitude, (C) PFM phase, (D) superimposed topography and amplitude, and (E) superimposed topography and phase.

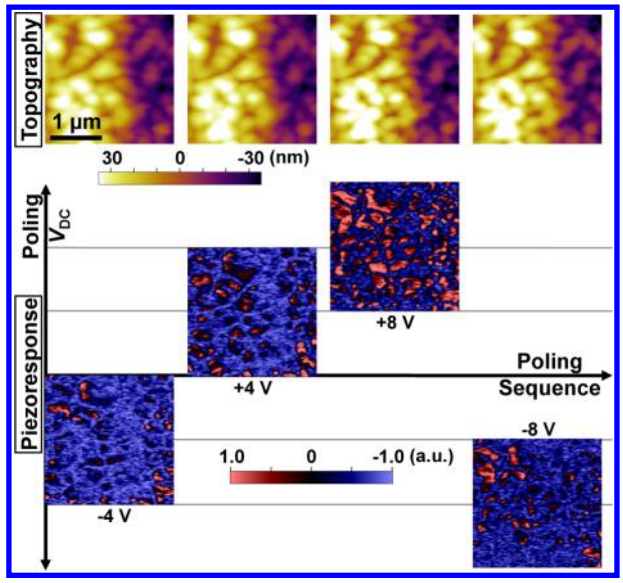

Figure 3. Four AFM topography images (top row) of a single 2.5 × 2.5 μm^2 area, with simultaneously acquired corresponding PFM images beneath mapping the $A{\cdot}\sin(\varphi)$ piezoresponse, each after scanned DC poling at the biases indicated (V_{DC}), evincing partial, reversible ferroelectric domain switching in as-processed β-$MAPbI_3$ thin film.

the local magnitude and orientation of the sample slope and curvature. Thus, Figure 2 provides, for the first time, direct evidence for the presence of ferroelectric domains in β-$MAPbI_3$ perovskite thin films.

The average domain size in the PFM images (Figures 2B and 2C) appears to be ∼100 nm, which is about the average size of the grains (Figure 1C). The conductive probes (contact mode) used in PFM are not as sharp compared to those used in conventional AFM, somewhat limiting spatial resolution of a given surface morphology, though sub-10 nm contact areas are expected for flat regions based on the imaging conditions. With this in mind, individual domains appear to correspond with individual grains in the β-$MAPbI_3$ thin films.

Figure 3 presents results from an experiment aimed at poling the ferroelectric domains in a β-$MAPbI_3$ thin film. The top row in Figure 3 presents height images (topography) of a single 2.5 × 2.5 μm^2 area, repeatedly scanned with AFM. Underneath each topography image is a simultaneously acquired corresponding PFM piezoresponse map, each obtained after a prior scan that poled the same area with pure DC bias (as labeled). To present the ferroelectric domains most clearly, $A{\cdot}\sin(\varphi)$ is displayed, where A is the amplitude and φ is the phase, in which case domains oriented into or out of the surface exhibit opposite amplitudes of piezoactuation (i.e., out of phase for the typical ±90° shift). The PFM images in Figure 3, which are positioned according to the prior poling DC bias in order to visually depict the poling sequence, are acquired without any applied DC bias to minimize capacitive artifacts.[23]

Throughout this experiment of more than eight consecutive scans, there is little evidence of specimen damage according to the nearly identical topography images (top row). This is despite the relatively soft nature of the β-$MAPbI_3$ thin films, which can be prone to deformation under the probe tip, especially in contact-mode imaging as required by PFM. The piezoresponse, on the other hand, is absolutely influenced by the poling DC bias magnitude and polarity. Compared to the initial image that followed DC poling with −4 V, several domains switch upon application of +4 V to the entire area. More domains then switch following the application of a larger DC bias of +8 V. After applying −8 V DC bias, many of these domains switch back to their original orientation. This is highlighted more clearly in the table-of-contents figure, which presents the difference in PFM phase contrast between these two extreme conditions (+8 V → −8 V). Of course, this applied DC bias is much larger than that used in the operation of perovskite-based solar cells, although the actual field applied across the film may be lower by a factor of two or more due to the tip−sample junction, as is common in PFM measurements.

As has been recently reported in other materials,[24] PFM-like contrast can sometimes occur due to electrochemical phenomena. This might be caused by, or lead to, modification of the specimen surface, local changes in the dielectric constant, ionic motion, etc. However, these mechanisms are typically accompanied by a significant change in topography, and/or relaxation of the topographic and/or PFM signals on the order of hundreds of seconds. Here, the topography remains unchanged throughout Figure 3 (top row). Furthermore, the time between DC poling and PFM imaging of any given region ranges from 2 to 1024 s from top to bottom of each consecutive scan, respectively. This is because full image acquisition times are on the order of 8 min, and sequential images are scanned in opposite y direction. Therefore, the evidence in Figure 3 supports the presence of ferroelectric domains in β-$MAPbI_3$ thin films. Furthermore, the ability to manipulate the domain orientation could possibly be used to influence photovoltaic performance in future work.

This experimental demonstration of the presence of ferroelectric domains in β-$MAPbI_3$ thin films and their reversible switching has several implications, some of which are discussed below.

dx.doi.org/10.1021/jz501697b | J. Phys. Chem. Lett. 2014, 5, 3335−3339

Based on some theoretical work, Frost et al.[15,18] hypothesize that polarized ferroelectric domains within the β-$MAPbI_3$ film may act as small internal $p-n$ junctions, aiding the separation of photoexcited electron and hole pairs. They suggest that the segregated paths ("ferroelectric highways") for electrons and holes provided by a distribution of these internal $p-n$ junctions would reduce recombination as the charge carriers travel across the thin film.[18] They also postulate that these effects could be responsible for the observed hysteresis and degradation of the photovoltaic performance in β-$MAPbI_3$-based solar cells.[18] Note that these hypotheses are based on the existence of extremely small domains (several unit cells wide).[18] However, the ferroelectric domains in β-$MAPbI_3$ thin films we observe in this first report are relatively large (~100 nm). Further work is needed to see if finer subgrain domains can be resolved in these hybrid perovskite thin films and if the hypothesized local $p-n$ junctions exist.

Juárez-Pérez et al.[10] have demonstrated experimentally giant dielectric constant (GDC) effect in β-$MAPbI_3$ thin films, where an already high dielectric constant (low-frequency) of 1000 increases by a factor of 1000 under 1 sun illumination. The presence and switching of the ferroelectric domains could play an important role in unraveling the mechanisms responsible for the observed GDC effect in these thin films.

Finally, Kim et al.[25] have performed a theoretical investigation of Rashba band splitting in β-$MAPbI_3$, where they show that polarization can be switched by external electric fields. This enables a controllable Rashba effect, providing the possibility of exploiting both spin and orbital freedom degrees in photoinduced effects in β-$MAPbI_3$.[25] Thus, the reversible switching of ferroelectric domains in β-$MAPbI_3$ thin films demonstrated here could also have implications in this regard.

In summary, ferroelectric domains are observed directly for the first time in solution-processed, high-quality β-$MAPbI_3$ thin films using piezoforce microscopy. The domains are approximately equal in size to the grains (~100 nm). Reversible ferroelectric domain switching has also been achieved by poling with DC biases. These experimental results encourage further investigations into the local ferroelectric behavior of hybrid perovskites, in particular through *in situ* characterization of photoeffects, as well as exploring domain engineering. Such investigations could yield new insights into the fundamental photovoltaic mechanisms for perovskite-based solar cells, potentially suggesting routes to enhance the performance of this promising class of novel photovoltaics.

■ ASSOCIATED CONTENT

Supporting Information

All the experimental procedures involving synthesis, characterization, and PFM are provided in the Supporting Information. This material is available free of charge via the Internet http://pubs.acs.org.

■ AUTHOR INFORMATION

Corresponding Authors

*E-mail: bhuey@ims.uconn.edu (B.D.H.).
*E-mail: nitin_padture@brown.edu (N.P.P.).

Author Contributions

‖(Y.K., L.Y., Y.Z.) These authors contributed equally.

Notes

The authors declare no competing financial interest.

■ ACKNOWLEDGMENTS

Y.Z. and N.P.P. thank the NSF (Grant No. DMR-1305913) for financial support, and Dr. H.F. Garces for experimental assistance. The PFM work by Y.K. and L.Y. is supported by DOE-BES-ESPM (Grant No. DE-SC0005037). B.D.H. acknowledges support from the iNano Visiting Professor program, Aarhus University, Denmark.

■ REFERENCES

(1) Service, R. F. Perovskite Solar Cells Keep on Surging. *Science* **2014**, *344*, 458.
(2) Mcgehee, M. D. Materials Science: Fast-Track Solar Cells. *Nature* **2013**, *501*, 323−325.
(3) Hodes, G. Perovskite-Based Solar Cells. *Science* **2013**, *342*, 317−318.
(4) Kim, H. S.; Im, S. H.; Park, N.-G. Organolead Halide Perovskite: New Horizons in Solar Cell Research. *J. Phys. Chem. C* **2014**, *118*, 5615−5625.
(5) Snaith, H. J. Perovskites: The Emergence of a New Era for Low-Cost, High-Efficiency Solar Cells. *J. Phys. Chem. Lett.* **2013**, *4*, 3623−3630.
(6) Zhou, H.; Chen, Q.; Li, G.; Luo, S.; Song, T.-B; Duan, H.-S; Hong, Z.; You, J.; Liu, Y.; Yang, Y. Interface Engineering of Highly Efficient Perovskite Solar Cells. *Science* **2014**, *345*, 542−546.
(7) Xing, G.; Mathews, N.; Sun, S.; Lim, S. S.; Lam, Y. M.; Grätzel, M.; Mhaisalkar, S.; Sum, T. C. Long-Range Balanced Electron and Hole-Transport Lengths in Organic-Inorganic $CH_3NH_3PbI_3$. *Science* **2013**, *342*, 344−347.
(8) Wolf, S. D.; Holovsky, J.; Moon, S.-J.; Löper, P.; Niesen, B.; Ledinsky, M.; Haug, F.-J.; Yum, J.-H.; Ballif, C. Organometallic Halide Perovskites: Sharp Optical Absorption Edge and Its Relation to Photovoltaic Performance. *J. Phys. Chem. Lett.* **2014**, *5*, 1035−1039.
(9) Savenije, T. J.; et al. Thermally Activated Exciton Dissociation and Recombination Control the Organometal Halide Perovskite Carrier Dynamics. *J. Phys. Chem. Lett.* **2014**, *5*, 2189−2194.
(10) Juárez-Pérez, E. J.; Sánchez, R. S.; Badia, L.; Garcia-Belmonte, G.; Kang, Y. S.; Mora-Sero, I.; Bisquert, J. Photoinduced Giant Dielectric Constant in Lead Halide Perovskite Solar Cells. *J. Phys. Chem. Lett.* **2014**, *5*, 2390−2394.
(11) Tan, Z.-K.; et al. Bright Light-Emitting Diodes Based on Organometal Halide Perovskite. *Nat. Nanotechnol.* **2014**, *9*, 687−692.
(12) Stoumpos, C. C.; Malliakas, C. D.; Kanatzidis, M. G. Semiconducting Tin and Lead Iodide Perovskites with Organic Cations: Phase Transitions, High Mobilities, and Near-Infrared Photoluminescent Properties. *Inorg. Chem.* **2013**, *52*, 9019−9038.
(13) Lines, M. E.; Glass, A. M. *Principles and Applications of Ferroelectrics and Related Materials*; Oxford University Press: London, 2001.
(14) Edri, E.; Kirmayer, S.; Henning, A.; Mukhopadhyay, S.; Gartsman, K.; Rosenwaks, Y.; Hodes, G.; Cahen, D. Why Lead Methylammonium Tri-Iodide Perovskite-Based Solar Cells Require a Mesoporous Electron Transporting Scaffold (But Not Necessarily a Hole Conductor). *Nano Lett.* **2014**, *14*, 1000−1004.
(15) Frost, J. M.; Butler, K. T.; Brivio, F.; Hendon, C. H.; Schilfgaarde, M.; Walsh, A. Atomistic Origins of High-Performance in Hybrid Halide Perovskite Solar Cells. *Nano Lett.* **2014**, *14*, 2584−2590.
(16) Huang, H. T. Solar Energy: Ferroelectric Photovoltaics. *Nature Photonics.* **2010**, *4*, 134−135.
(17) Snaith, H. J.; Abate, A.; Ball, J. M.; Eperon, G. E.; Leijtens, T.; Noel, N. K.; Stranks, S. D.; Wang, J. T.-W.; Wojciechowski, K.; Zhang, W. Anomalous Hysteresis in Perovskite Solar Cells. *J. Phys. Chem. Lett.* **2014**, *5*, 1511−1515.
(18) Frost, J. M.; Butler, K. T.; Walsh, A. Molecular Ferroelectric Contributions to Anomalous Hysteresis in Hybrid Perovskite Solar Cells. *APL Mater.* **2014**, *2*, 081506.

(19) Gruverman, A.; Auciello, O.; Tokumoto, H. Imaging and Control of Domain Structures in Ferroelectric Thin Films via Scanning Force Microscopy. *Annu. Rev. Mater. Sci.* **1998**, *28*, 101−123.
(20) Huey, B. D.; Premnath, R. N.; Lee, S.; Polomoff, N. A. High Speed SPM Applied for Direct Nanoscale Mapping of the Influence of Defects on Ferroelectric Switching Dynamics. *J. Am. Ceram. Soc.* **2012**, *95*, 1147−1162.
(21) Burschka, J.; Pellet, N.; Moon, S. J.; Humphrey-Baker, R.; Gao, P.; Nazeeruddin, M. K.; Grätzel, M. Sequential Deposition as a Route to High-Performance Perovskite-Sensitized Solar Cells. *Nature* **2013**, *499*, 316−319.
(22) Xiao, Z.; Bi, C.; Shao, Y.; Dong, Q.; Wang, Q.; Yuan, Y.; Wang, C.; Gao, Y.; Huang, J. Efficient, High Yield Perovskite Photovoltaic Devices Grown by Interdiffusion of Solution-Processed Precursor Stacking Layers. *Energy Environ. Sci.* **2014**, *7*, 2619−2623.
(23) Huey, B. D.; Ramanujan, C.; Bobji, M.; J. Blendell, J. E.; White, G.; Szoszkiewicz, R.; A. Kulik, A. The Importance of Distributed Loading and Cantilever Angle in Piezo-Force Microscopy. *J. Electroceram.* **2004**, *13*, 287−291.
(24) Kalinin, S. V.; Jesse, S.; Tselev, A.; Baddorf, A. P.; Nina, B. The Role of Electrochemical Phenomena in Scanning Probe Microscopy of Ferroelectric Thin Films. *ACS Nano* **2011**, *5*, 5683−5691.
(25) Kim, M.; Im, J.; Freeman, A. J.; Ihm, J.; Jin, H. Switchable $S = 1/2$ and $J = 1/2$ Rashba Bands in Ferroelectric Halide Perovskites. *Proc. Natl. Acad. Sci. U. S. A.* **2014**, *111*, 6900−6904.